Journal of Magnetic Resonance **147,** 286–295 (2000)
doi:10.1006/jmre.2000.2190, available online at http://www.idealibrary.com on IDEAL®

On the Conversion of Triple- to Single-Quantum Coherences in MQMAS NMR

M. Pruski,*[,1] J. W. Wiench,* and J.-P. Amoureux†

*Ames Laboratory, Iowa State University, Ames, Iowa 50011; and †Université de Lille-1, F-59655 Villeneuve d'Ascq Cedex, France

Received May 8, 2000; revised July 31, 2000

A systematic experimental and numerical evaluation of several basic approaches to multiple-quantum magic angle spinning (MQMAS) NMR is presented for spin-$\frac{3}{2}$ nuclei. The approaches use identical MQ excitation, via a single RF pulse of high power, and three types of methods for conversion to observable coherence: (a) nutation by strong continuous wave pulse; (b) rotation-induced adiabatic coherence transfer (RIACT), and (c) fast amplitude modulation (FAM-1). The optimization strategies and maximum achievable MQMAS efficiencies of ^{87}Rb in $RbNO_3$ and $LiRbSO_4$ are investigated using several coherence transfer schemes under a wide range of experimental parameters. These parameters include the strength of the RF magnetic field ν_{RF}, the sample rotation speed ν_R, the length of the conversion period, and the modulation frequency in FAM-1. The data provide new insights into the spin dynamics involved in these techniques and the experimental guidelines for achieving the best sensitivity. The RF requirements for maximum efficiency of conversion depend on the method to be used. In general, FAM-1 performs better than the nutation and RIACT methods in terms of efficiency and off-resonance behavior, especially when ν_{RF} is small compared to the quadrupole frequency ν_Q. The experiments performed using nutation, RIACT, and FAM-1 methods yield similar resolution in the isotropic dimension, regardless of ν_{RF}. © 2000 Academic Press

Key Words: **quadrupole nuclei; multiple quantum MAS NMR; efficiency of conversion.**

INTRODUCTION

Following its discovery in 1995 by Frydman and colleagues (*1, 2*), multiple-quantum magic angle spinning (MQMAS) became the method of choice for acquiring isotropic spectra of half integer quadrupolar nuclei with the quadrupolar coupling constant C_Q in the megahertz range. Complete averaging of the second-order broadening in such nuclei was earlier accomplished by rotating the sample about time-dependent axes in double rotation (*3*) and dynamic angle spinning (*4*) experiments. MQMAS eliminates the quadrupolar broadening by fixing the rotor orientation at the magic angle (54.7° with respect to the magnetic field) and by changing the coherence order p during the course of a two-dimensional experiment. In addition, sample spinning at the magic angle eliminates the chemical shift anisotropy and reduces the dipolar interactions. The MQMAS experiment correlates the phase evolutions of the p-quantum coherence in t_1 and the single-quantum coherence in t_2 by generating a purely isotropic echo at

$$t_{2e} = R(S, p)t_1, \qquad [1]$$

where $R(S, p)$ is a known function of the nuclear spin S and p.

MQMAS is technically straightforward and consequently found numerous applications in the studies of catalysts (*5–7*), glasses (*8, 9*), and other amorphous and crystalline inorganic solids (*10, 11*). However, considerable research effort was focused on further developments of the method itself. Specifically targeted in these investigations was the main weakness of MQMAS, namely the limited efficiency of excitation of multiple-quantum coherence (MQC) and its conversion to the observable single-quantum coherence (SQC). It quickly became clear that the overall efficiency of MQMAS is mainly controlled by the conversion step (*12*). Both numerical simulations and experimental results have shown that efficient excitation of the MQC can be simply achieved with a single, continuous wave (CW) short pulse of high intensity. The excitation schemes that used two pulses, composite pulses and shaped pulses, produced, at best, only a small additional gain of signal-to-noise ratio (S/N) (*13–15*). On the other hand, the efficiency of conversion processes could be significantly increased by using the highest possible RF field (*16*), fast amplitude modulation (FAM) (*17, 18*), or double frequency sweeps that cover the satellite transitions of all crystallites in a powder (*19*). The FAM method, which follows the concept used earlier by Vega and Naor (*20*), is of special interest, as it is easy to implement in standard NMR spectrometers.

In the absence of large offset, the response of quadrupolar spins to RF excitation depends mainly on the relative magnitudes of ν_{RF} and the quadrupole splitting $\bar{\nu}_Q$. This splitting is given by

$$\bar{\nu}_Q(\alpha_s, \beta_s, \eta_Q) = 1.5\nu_Q[3\cos^2\beta_s - 1 + \eta_Q\sin^2\beta_s\cos 2\alpha_s], \qquad [2]$$

[1] To whom correspondence should be addressed at 230 Spedding Hall, Ames Laboratory, Iowa State University, Ames, IA 50011. Fax: (515) 294-5233. E-mail: mpruski@iastate.edu.

1090-7807/00 $35.00

where $\nu_Q = C_Q/4S(2S - 1)$ is the quadrupole frequency, η_Q is the asymmetry parameter, and the angles α_s and β_s describe the orientation of the magnetic field $\mathbf{B}_0$ in the principal axis system of the electric field gradient tensor. As a result, the MQMAS efficiency varies with the crystallite orientation in a powdered sample and spectral distortions are likely to occur in the anisotropic dimension. The relative intensities observed along the isotropic dimension are also skewed, as the same mechanism is responsible for uneven excitation of different sites in a sample. Several strategies have been proposed to remedy this problem. Some of them rely upon numerical simulations of the MQMAS spectra. For example, the isotropic chemical shifts and quadrupolar induced shifts obtained from MQMAS can be utilized in the computer simulations of one-dimensional, quantitative MAS spectra in order to obtain the remaining lineshape parameters, including their relative intensities (*8*). More advanced techniques involve complete quantitative determination of quadrupolar and chemical shift parameters via direct simulation of MQMAS spectra (*21, 22*). Other methods for quantitative detection use the excitation and conversion schemes that are less sensitive to the magnitude of the quadrupole splitting, especially in experiments involving triple-quantum coherence (TQC) of spin-$\frac{3}{2}$ muscles. Rotation-induced adiabatic coherence transfer (RIACT) (*23*), as well as the FAM-1 (*17, 18*) experiment mentioned previously, fall into this category. Both methods can achieve TQC $\rightarrow$ SQC transfer under magic angle spinning when $\bar{\nu}_Q$, given by Eq. [2], becomes time dependent and oscillates back and forth between its extreme values of the order of $\pm\nu_Q$. Efficient TQC $\rightarrow$ SQC conversion requires that these changes are adiabatic, i.e., slow enough that the spins continuously follow the eigenstates of the Hamiltonian. Vega introduced the following, practical definition of the adiabaticity parameter (*24*):

$$\alpha_{ad} = \nu_{RF}^2/6\,\nu_Q\nu_R. \qquad [3]$$

The adiabaticity parameter must satisfy the condition $\alpha_{ad} \gg 1$ for the passage to be characterized as adiabatic. For the $\alpha_{ad} \ll 1$ case, referred to as sudden passage, the spins remain in their original eigenstates during MAS. In addition to these developments, numerous pulse schemes and coherence transfer pathways were devised to obtain pure absorption MQMAS lineshapes (*25–27*).

Given the multitude of available pulse sequences, coherence pathways, and acquisition schemes, the choice of which way to carry out the MQMAS experiment is often uncertain. While the performance of various methods has been demonstrated for a number of samples under selected experimental conditions (*12, 17, 18, 23, 26, 28*), a general comparison of MQMAS schemes is difficult to make due to the incompleteness and the incompatibility of the existing data. In this work, we present a systematic experimental and numerical study of the basic methods used in the TQC $\rightarrow$ SQC conversion in spin-$\frac{3}{2}$ nuclei. While the primary purpose of this study is the efficiency, we also investigate the sensitivity to C_Q and the resolution in the isotropic dimension. The effect of several experimental parameters is investigated, including the shape and length of the conversion pulse(s), the magnitude of the RF field ν_{RF}, and the sample rotation rate ν_R. Patterns for optimizing the experimental strategy in MQMAS are shown, which are mainly dictated by relative sizes of ν_{RF} and ν_Q. It is emphasized that most of the spectral intensities reported in this work include contributions from both echo ($0 \rightarrow -3 \rightarrow \ldots$) and antiecho ($0 \rightarrow +3 \rightarrow \ldots$) coherence pathways. The second-order lineshapes and the interplay between echo and antiecho intensities will be scrutinized in a separate study.

EXPERIMENTAL

The experimental data were mostly obtained using 3QMAS NMR of ^{87}Rb in rubidium nitrate ($RbNO_3$). This is a popular test compound in MQMAS NMR (*25, 26, 28–30*), and we will refer to some of the earlier results in the discussion. $RbNO_3$ was obtained from Aldrich and was used without further purification. The quadrupole coupling constant C_Q, the asymmetry parameter η_Q, and the isotropic chemical shift δ_{CS} (with respect to an aqueous $RbNO_3$ solution) of the three Rb sites in $RbNO_3$ are as follows: Rb_1 (1.7 MHz, 0.2, -27 ppm), Rb_2 (2.0 MHz, 1.0, -28 ppm), and Rb_3 (1.8 MHz, 0.5, -31 ppm) (*25*). Several spectra were also recorded with crystalline lithium rubidium sulfate ($LiRbSO_4$), which at room temperature exhibits a single ^{87}Rb line with a larger C_Q value of 5.35 MHz (*31*).

The basic approaches to MQMAS examined in this study use four types of coherence transfer pathways: $0 \rightarrow \pm3 \rightarrow -1$, $0 \rightarrow +3 \rightarrow +1 \rightarrow -1$, $0 \rightarrow \pm3 \rightarrow 0 \rightarrow -1$, and $0 \rightarrow \pm3 \rightarrow \pm1 \rightarrow 0 \rightarrow -1$. We will refer to them, for brevity, as schemes I, II, III, and IV, respectively. One additional experiment derived from scheme IV utilized the pathway $0 \rightarrow \pm3 \rightarrow \pm1 \rightarrow 0 \rightarrow +1 \rightarrow -1$ (scheme IV′). Schematic diagrams of the RF sequences used and the corresponding coherence transfer pathways are shown in Fig. 1. Scheme I has been introduced in the initial studies (*2, 5, 32*). Scheme II is used in the split-t_1/shifted echo experiment (*25, 26, 33, 34*). The split-t_1 method redefines the t_1 domain in order to eliminate the need for shearing, whereas the shifted echo method can improve the S/N ratio and yields pure absorption spectra. Schemes III and IV feature symmetric pathways $0 \rightarrow \pm3 \rightarrow 0$ and $0 \rightarrow \pm3 \rightarrow \pm1 \rightarrow 0$, respectively. They are followed by selective $\pi/2$ pulses, which complete the so-called z-filter (*27, 35*). This symmetrization of pathways allows for simultaneous acquisition of the echo and antiecho signals with equal intensity, which leads to cosine modulated FIDs and thus to pure absorption phase spectra. Scheme III does not use a direct TQC $\rightarrow$ SQC conversion and is commonly applied as shown in Fig. 1. Scheme IV is used in the split-t_1 experiment (*35*) and can be further combined with the shifted echo (scheme IV′) (*26*).

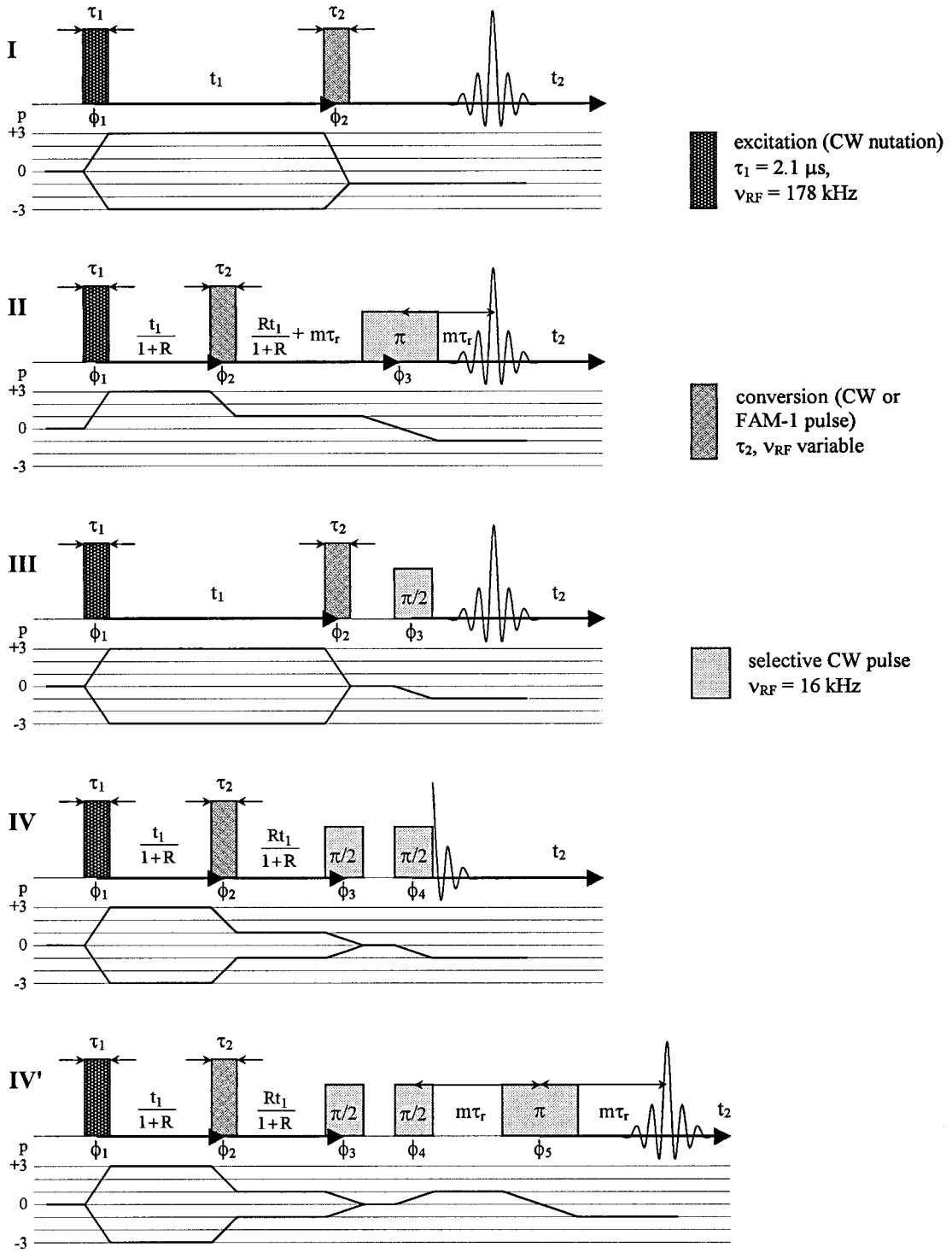

FIG. 1. Pulse sequences and coherence transfer pathways used in this work: standard two-pulse experiment (I), split-t_1/whole echo experiment (II), simple z-filtered experiment with symmetric pathway (III), split-t_1 experiment (IV), and its whole echo extension (IV′). The ν_{RF} values were 178 kHz for the first (excitation) pulse and 16 kHz for the selective π and $\pi/2$ pulses.

To reduce the number of variable parameters, the excitation of TQC was always achieved with a single pulse of duration $\tau_1 = 2.1$ μs and the RF field $\nu_{RF} = 178$ kHz, whereas the selective pulses for single quantum transitions used $\nu_{RF} = 16$ kHz. The time delay between the second and third pulses in scheme III and between the two $\pi/2$ pulses in schemes IV and

IV′ was always 0.2 ms. The conversion step used CW (nutation and RIACT-I) and FAM-1 pulses that varied in terms of duration τ_2 and power ν_{RF}. The FAM-1 pulse sequence included n sections of alternating RF pulses $\nu_{RF}(\varphi)$–0–$\nu_{RF}(\varphi + \pi)$–0 (where φ denotes the pulse phase), with each level turned on for an equal period of time τ_{AM}. Thus, the overall duration τ_2 of the FAM-1 sequence was equal to $4n\tau_{AM}$ with the corresponding irradiation frequency components $\pm\nu_{AM}$ and $\pm 2\nu_{AM}$, where $\nu_{AM} = (4\tau_{AM})^{-1}$. We note that the rise time and fall time of the RF pulses received by the probe used in this work were of the order of 0.3 μs, which may have affected the experimental data obtained with $\tau_{AM} < 0.5$ μs.

All spectra were recorded at room temperature on a Chemagnetics Infinity spectrometer operating at 130.88 MHz. This frequency matched the first moment of the MAS lineshape in $RbNO_3$. The spectrometer was equipped with a 3.2-mm Varian/Chemagnetics MAS probehead, which employed sample rotation rates between 5 and 20 kHz. For all schemes, the overall intensity of the 2D spectrum was simply determined as the magnitude of the signal resulting from Fourier transform of the cosine and sine components of the first row of hypercomplex data. In selected cases, complete two-dimensional MQMAS spectra were obtained to evaluate the resolution.

The behavior of ^{87}Rb spins in a rotating sample was simulated using the homemade program PULSAR (*36*). This program provides a powder-averaged analysis of the spin dynamics involved in various experiments by propagating the spin density matrix under relevant Hamiltonians, which in this case included the first- and second-order time-dependent quadrupolar interactions and the RF fields. In agreement with the experimental data, the reported intensities are equal to the modulus of the $(-\frac{1}{2}, \frac{1}{2})$ coherence at $t_1 = 5$ μs. Two important assumptions were made to accelerate the numerical analysis. First, a single set of values was used in $RbNO_3$: $C_Q = 2.0$ MHz and $\eta_Q = 0$. With the quadrupolar interactions for Rb_1, Rb_2, and Rb_3 in $RbNO_3$ being similar, this assumption has a negligible effect on the main conclusions of this work. Second, the simulations did not account for inhomogeneity of the RF field across the sample. Most likely, this is the largest source of discrepancy between the experiment and the simulations.

All figures presented in this study show the total Rb intensity in the sample normalized with respect to the maximum signal that can be obtained in a conventional MAS experiment using a selective excitation of the central transition by a 90° pulse.

RESULTS AND DISCUSSION

General Considerations

The spin dynamics involved in the TQC → SQC conversion under FAM-1 and CW conditions has recently been studied by Madhu *et al.* (*18*). Their analytical approach involved fictitious spin-$\frac{1}{2}$ operator formalism, which expresses the spin states and operable Hamiltonians in terms of angular momentum operators $\{I_\alpha^{rs}\}$, where $\alpha = x, y, z$ and r, s denote the energy eigenstates of the quadrupolar Hamiltonian: $|1\rangle = |\frac{3}{2}\rangle, \ldots, |4\rangle = |-\frac{3}{2}\rangle$. The dynamics of the TQC → SQC conversion process can be described as (*18*)

$$I_x^{14} \rightarrow c_{xx}(t)I_x^{23} + c_{xy}(t)I_y^{23},$$
$$I_y^{14} \rightarrow c_{yy}(t)I_y^{23} + c_{yx}(t)I_x^{23}, \qquad [4]$$

where the coefficients $c_{xx}(t)$ and $c_{xy}(t)$ represent the amount of SQC I_x^{23} and I_y^{23} created from TQC I_x^{14}, etc. In general, an efficient echo in MQMAS is obtained when (i) $c_{xx}(t)$ and $c_{yy}(t)$ are maximized, (ii) $c_{xx}(t) = \pm c_{yy}(t)$ (the sign depends on the coherence pathway selection), and (iii) $c_{xy}(t) = c_{yx}(t) = 0$.

In the static sample, the FAM-1-driven TQC → SQC conversions will occur only in those crystallites for which the modulation rate of RF matches the quadrupole splitting. Under MAS, the anticrossing of energy levels can take place for each nucleus that undergoes the spinning-induced resonance condition. Under the adiabatic FAM conversion, this condition requires that $\bar{\nu}_Q = \pm\nu_m$ or $\pm 2\nu_m$ and results in efficient $I_{x,y}^{14} \rightarrow I_{x,y}^{23}$ transfer with $c_{xx}(t) = c_{yy}(t) = 1$ and no intermixing ($c_{xy}(t) = c_{yx}(t) = 0$) (*18*). In the presence of off-resonance modulation and second-order quadrupolar effects the transfer is not complete and intermixing becomes possible ($c_{xy}(t) \neq 0 \neq c_{yx}(t)$). While the CW irradiation also induces the $I_{x,y}^{14} \rightarrow I_{x,y}^{23}$ transfers, the efficiencies of $I_x^{14} \rightarrow I_x^{23}$ and $I_y^{14} \rightarrow I_y^{23}$ processes are not equal. More importantly, however, severe oscillations of one of the magnetization components are expected in this case. These oscillations should have a detrimental effect on the formation of the echo in MQMAS experiments that use long-pulse CW conversion, as is the case in the RIACT scheme.

The analysis of rotating powders is very complex. As we mentioned earlier, the magnitude of quadrupole splitting varies widely depending on the orientation of a crystallite. This causes a complex nutation behavior of quadrupolar spins during excitation and conversion pulses, as $\bar{\nu}_Q$ can be much larger, much smaller, or comparable to ν_{RF} (e.g., $\bar{\nu}_Q = 3\nu_Q$ for $\alpha_s = \beta_s = 0$, and $\bar{\nu}_Q = 0$ for $\alpha_s = 45°$ and $\beta_s = 54.74°$, see Eq. [2]) depending on the crystallite orientation. In addition, a sharp distinction between sudden and adiabatic anticrossing cases cannot be made in a powdered sample. Under most experimental conditions this distinction has only a statistical meaning, as significant fractions of crystallites undergoing adiabatic and sudden passages may coexist in the sample. Further complications arise from the fact that TQC → SQC are not the only transfers used in MQMAS, as is the case in scheme III. Also, different coherence transfer mechanisms and pathways can compete in a single experiment, as will be demonstrated later. Finally, most schemes utilize both echo and antiecho pathways, which can interfere constructively or destructively under various experimental conditions. It is thus imperative to use numerical simulations of the evolution of the spin density matrix to obtain the powder-averaged efficiency curves for MQMAS.

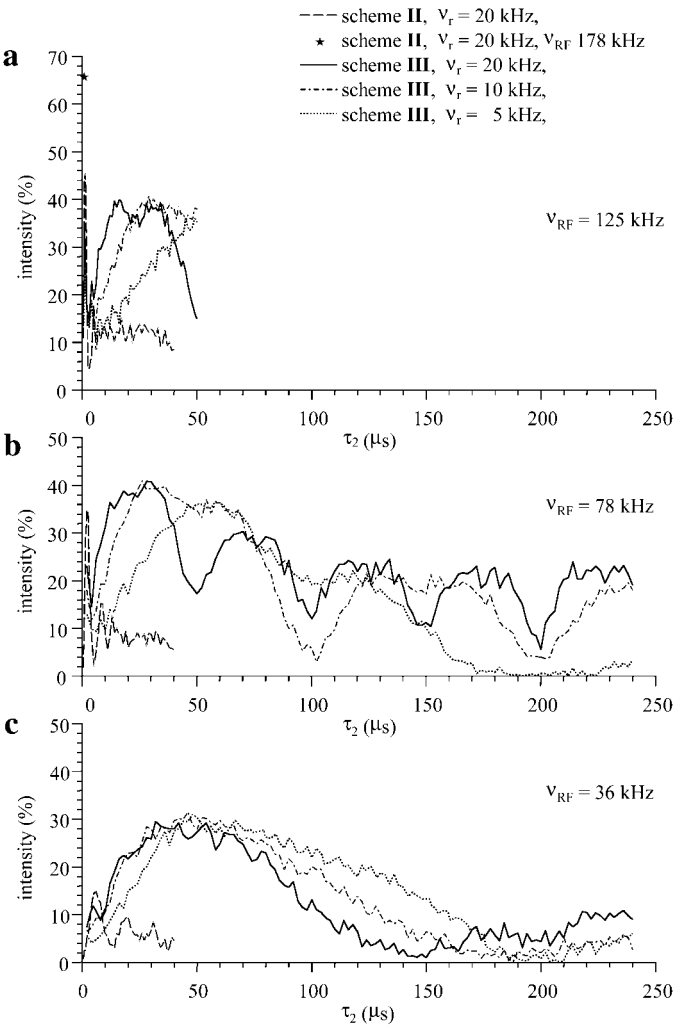

FIG. 2. Efficiency of schemes III and IV in $RbNO_3$ versus τ_2 in the range $0 < \tau_2 < 240$ μs: (a) $\nu_{RF} = 125$ kHz, (b) $\nu_{RF} = 78$ kHz, and (c) $\nu_{RF} = 36$ kHz. The dashed line represents scheme III, which used $\nu_R = 20$ kHz. The maximum intensity obtained with this scheme at $\nu_{RF} = 178$ kHz is shown with an asterisk. The dotted, dotted/dashed, and solid lines represent scheme IV with MAS rates $\nu_R = 5$, 10, and 20 kHz, respectively.

Optimization of CW and FAM-1 Conversions

We begin our discussion by examining Fig. 2, which shows the evolution of MQMAS intensities in $RbNO_3$ obtained experimentally for the symmetric schemes III and IV. Schemes I, II, and IV′, which all include direct TQC → SQC transfers, require a similar optimization strategy to scheme IV. The data were measured under CW conversion, for selected values of ν_{RF} (36, 78, 125, and 178 kHz) and ν_R ($\nu_R = 5$, 10, and 20 kHz). For $\nu_{RF} \leq 78$ kHz, a long time scale of $0 < \tau_2 < 240$ μs has been chosen to monitor the change of magnetization over several rotor periods. In order to protect our MAS probe, we limited τ_2 to 50 μs at $\nu_{RF} = 125$ kHz and to 2 μs at $\nu_{RF} = 178$ kHz. A closer view of the initial 30 μs of the evolution and the corresponding simulations is shown in Fig. 3. It is noted that the efficiency of TQC excitation depends on the sample rotation rate. According to the simulations, a 2.1-μs pulse with $\nu_{RF} = 178$ kHz results in TQC intensity of 148, 144, and 130% for $\nu_R = 5$, 10, and 20 kHz, respectively. This decrease of intensity has been explained in an earlier study (*16*).

Generally, there is a satisfactory qualitative and quantitative agreement between the measured and calculated curves. This validates both the experiment and the theory and allows us to discuss these results jointly hereafter.

Figures 2 and 3 show that for both CW methods the overall efficiency of MQMAS in $RbNO_3$ increases with increasing ν_{RF}, regardless of the spinning conditions. This is in agreement with previous studies (*12, 16*), as the condition $\nu_{RF} \leq \nu_Q$ applies here. However, the efficiencies observed using schemes III and IV evolve in sharply different ways. Scheme IV yields the intensities that are modulated coherently with the rotor period τ_R when the RF field is sufficient to fulfill the adiabaticity criterion for most crystallites (see Fig. 2b). This phenomenon results from the RIACT effect between TQC and SQC coherences (*23, 24*). The three-pulse sequence used in scheme III produced very different results. The observed signal shows faster and deeper oscillations. Since the frequency corresponding to these oscillations is equal to $2\nu_{RF}$, (i.e., to the nutation frequency of the spins $\frac{3}{2}$), they are interpreted as the result of a continuous transfer between zero- and single-quantum coherence states. These oscillations decay to zero within one rotor period. It is noted that this oscillatory behavior is also superimposed on the initial part of the curves for scheme IV, where it competes with the RIACT phenomenon. The initial behavior of magnetization observed in this case is consistent with the earlier study that used the two-pulse sequence without *z*-filter, i.e., the nutation coherence transfer pathway of type I (*12*).

As a result of these phenomena, the experiments involving schemes III and IV require different optimization strategies. For $\nu_{RF} < 100$ kHz, scheme IV performs best with τ_2 between $\tau_R/4$ and $\tau_R/2$, i.e., when the conversion time is sufficiently long to allow for an efficient RIACT mechanism to become operative. The RIACT effect is especially evident in Fig. 2b. This conclusion is consistent with a recent study by Larsen and Nielsen (*29*), who found similar optimized conditions in an experiment that utilized the $0 \rightarrow \pm 3 \rightarrow \pm 1$ pathway followed by the quadrupolar echo and Carr–Purcell–Meiboom–Gill sequence. However, at high RF fields, the initial burst of intensity due to CW nutation maximizes the efficiency (see Fig. 3a). Our results also validate earlier recommendations of using short pulses in the sequences that utilize scheme III (*12, 32*). The maximum efficiencies achievable with these methods and the optimized conditions are given in Table 1, which will be discussed later in this work.

The representative results of the FAM-1 experiment in $RbNO_3$ are shown in Fig. 4. Since this method results mainly in the TQC → SQC conversion, initial experiments were performed using schemes II and IV. The search for best efficiency was carried out in a three-dimensional space of variable parameters, which included ν_{RF}, τ_{AM}, and the number of mod-

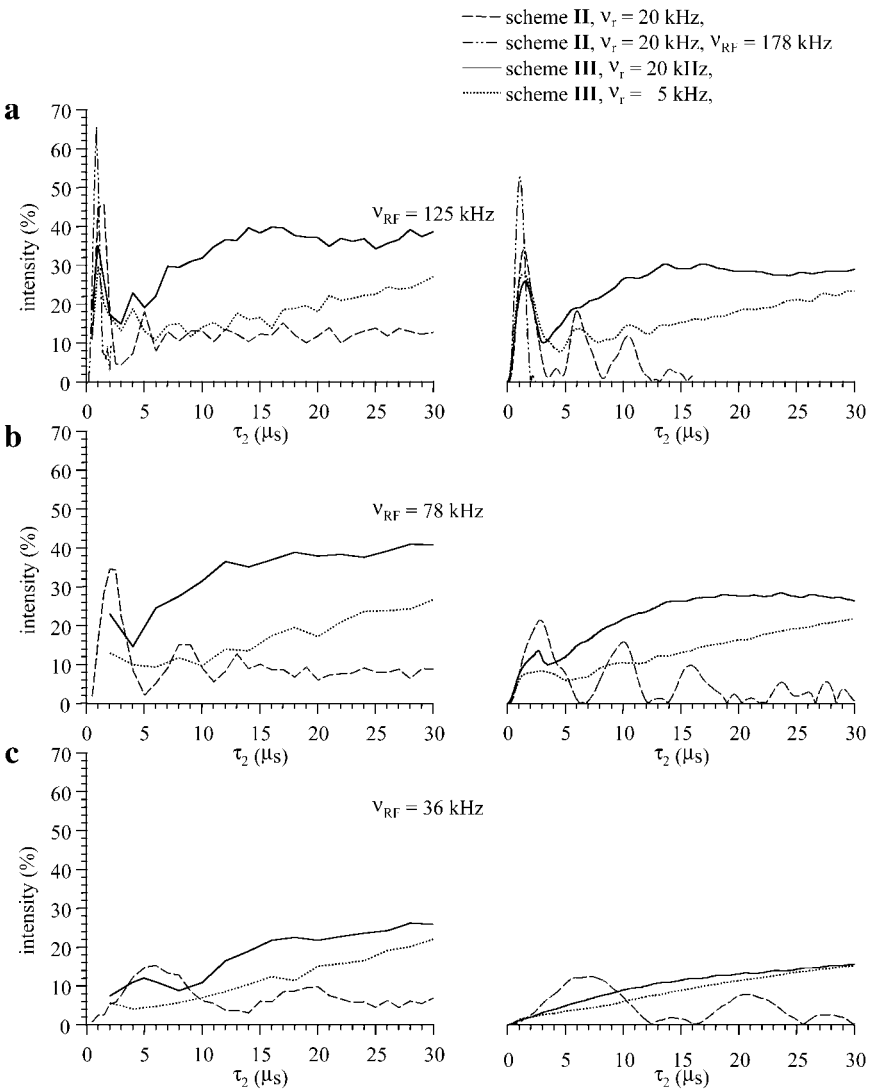

FIG. 3. The experimental data of Fig. 2 (left column) are compared with the corresponding density matrix simulations (right column) in the range $0 < \tau_2 < 30$ μs. The dashed line represents experiment III performed with MAS rate $\nu_R = 20$ kHz; the dotted and solid lines were obtained with scheme IV using $\nu_R = 5$ and 20 kHz, respectively. The double dotted/dashed line in (a) represents experiment III performed with $0 < \tau_2 < 5$ μs and $\nu_{RF} = 178$ kHz.

ulation blocks n. Two examples of the observed dependencies are shown in Fig. 4. Figure 4a presents the total efficiency of the FAM-1 3QMAS experiment that utilized scheme IV, as a function of ν_{RF}. The curves were measured for $1 \leq n \leq 5$ and a constant modulation frequency $\nu_{AM} = 250$ kHz. The maximum intensity observed under these conditions varied between 54% for $n = 1$ (at $\nu_{RF} = 115$ kHz) and 56% for $n = 3$ (at $\nu_{RF} = 90$ kHz). The curves shown in Fig. 4b represent the efficiency of scheme II as a function of τ_{AM}, obtained for several values of ν_{RF} with $n = 3$. As was mentioned earlier, the maximum efficiency in FAM-1 is obtained when $\bar{\nu}_Q = \pm\nu_{AM}$ or $\pm 2\nu_{AM}$ (*18*). It is difficult to make a good estimate of τ_{AM} for a powder; however, values between 1 and 1.5 μs are expected for $RbNO_3$. Interestingly, Fig. 4b shows that the optimum value of τ_{AM} strongly depends on the magnitude of the RF field. For decreasing ν_{RF} values, the maximum intensity is measured at decreasing modulation frequencies. This behavior may result from (i) the effect of other coherence transfer mechanisms that compete with FAM-1, e.g., nutation in case of large ν_{RF}, and (ii) loss of adiabaticity during spinning-induced level crossing at lower values of ν_{RF}.

Despite these complications, the FAM-1 3QMAS experiment is surprisingly robust as the maximum intensity measured does not change significantly versus n or ν_{RF}. It is also noted that, for a given ν_{RF}, the optimized values of τ_{AM} are similar for all schemes used in this work (see Table 1).

Efficiency

The efficiencies of conversion using CW and FAM-1 methods in $RbNO_3$ are compared in Table 1 and Fig. 5. With the

TABLE 1
Optimized Nutation, RIACT, and FAM-1 Conversion Pulses as a Function of ν_{RF} and the Resulting MQMAS Intensities Measured in $RbNO_3$

Method	ν_{RF} (kHz)	τ_2 (μs)[a]	I_{max} (%) I	II	IV	IV′	τ_2 (μs)[a]	I_{max} (%) III
Nutation	178	0.65	75	56	44	34	0.85	66
	125	0.75	48	39	29	23	1.25	46
	104	1.1	44	35	26	20	1.4	35
	78	1.5	36	28	21	16	2.0	27
	60	2.2	29	22	16	13	3.0	22
	36	5.0	20	13	12	8	6.5	15
RIACT	125	18	84	48	37	27		
	104	18	87	48	36	28		
	78	18	85	49	37	29		
	60	25	80	48	35	26		
	36	50	61	34	28	20		
FAM-1	178	0.55	77	63	46	37	0.65	54
	125	0.65	82	69	52	40	0.85	52
	104	0.80	83	70	51	40	1.15	49
	78	1.15	79	67	49	39	1.95	45
	60	1.45	72	59	44	34	2.4	41
	36	3.2	56	44	36	27	4.6	36

[a] In the case of FAM-1, $\tau_2 = \tau_M$.

exception of scheme II, the intensities reported here include contributions from both echo ($0 \rightarrow -3 \rightarrow \ldots$) and antiecho ($0 \rightarrow +3 \rightarrow \ldots$) coherence pathways. For the symmetric schemes III, IV, and IV′, these two pathways provide equal intensities when selected separately, regardless of the conversion method. Nevertheless, when the echo and antiecho are acquired in one experiment, the observed signal can be less intense than the sum of its individual components acquired independently. This interplay between echo and antiecho becomes more complex in the nonsymmetric scheme I. When used with nutation or RIACT conversion, this scheme benefits from contributions from both pathways (*22*, *28*). Under properly optimized FAM-1 conversion, however, scheme I exhibits high selectivity toward the $0 \rightarrow -3 \rightarrow -1$ pathway. This feature of FAM has been earlier illustrated in Ref. (*28*). We also note that a delay $m\tau_R = 5$ ms was used for schemes II and IV′ in order to observe the whole echo. However, the intensities reported for these two schemes are based on the Fourier transformation of the half-echo signal. The same signal can be transformed starting at $t_2 = 0$ to yield, after appropriate linear phase correction, a spectrum that is almost twice as intense as would have been observed for $m\tau_R = 0$. Full signal recovery is not possible due to T_2 relaxation, which in the case of $RbNO_3$ and $m\tau_R = 5$ ms reduced the intensity by almost 15% ($T_2 \cong 66$ ms). Small additional losses can result from the imperfections of selective pulses. Note, however, that acquisition of the whole echo increases the noise level, by a factor of $\sqrt{2}$, as well. Thus, the data reported here for schemes II and IV′ should be multiplied by $\sqrt{2}$ to reflect the absolute S/N ratio achieved with these methods.

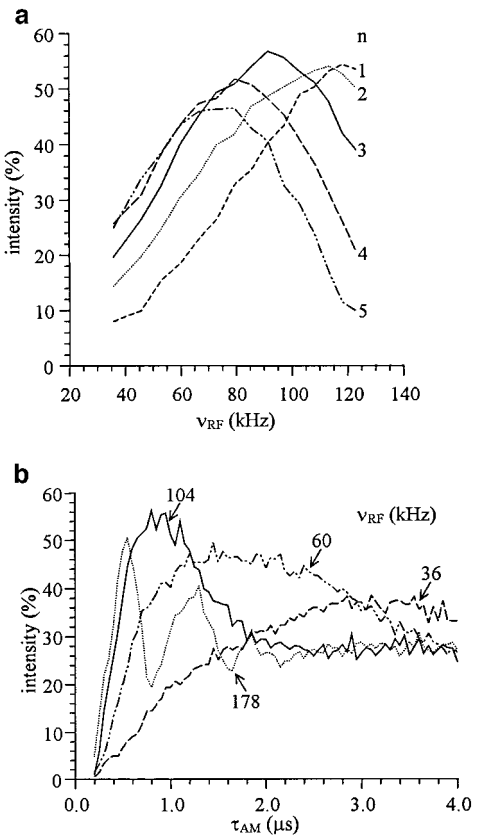

FIG. 4. Optimization of FAM-1 3QMAS experiment in $RbNO_3$ (experimental data). In (a), the total efficiency of scheme IV is shown versus ν_{RF} for $\tau_{AM} = 1$ μs and $1 \leq n \leq 5$, as marked. (b) Shows the total efficiency of scheme II versus τ_{AM} measured for $n = 3$ and several values of ν_{RF}, as marked.

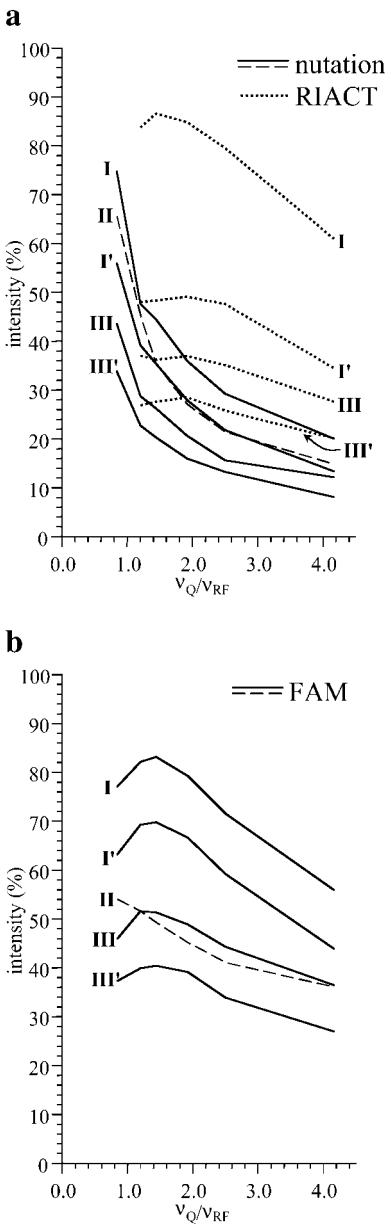

FIG. 5. Optimized MQMAS intensity of ^{87}Rb in $RbNO_3$ versus ν_Q/ν_{RF}, obtained experimentally with schemes I, II, III, IV, and IV′ using nutation, RIACT, and FAM-1 for TQC → SQC conversion. The excitation of triple-quantum coherences was achieved using a single CW pulse with $\tau_1 = 2.1$ μs and $\nu_{RF} = 178$ kHz, whereas the selective $\pi/2$ and π pulses used $\nu_{RF} = 16$ kHz. The ν_Q/ν_{RF} ratio was evaluated using an average C_Q value for $RbNO_3$: $\nu_Q = (1.8\ \text{MHz})/4S(2S - 1) = 150$ kHz. Note that schemes II and IV′ used the whole echo ($m\tau_R = 5$ ms). Since the reported intensities are based on Fourier transformation of the half-echo signal, the actual S/N ratio is underestimated by $\sqrt{2}$ for these two methods.

As mentioned previously, the excitation of triple-quantum coherences was accomplished by using a single nutation pulse with $\tau_1 = 2.1$ μs and $\nu_{RF} = 178$ kHz. A constant rotation rate ($\nu_R = 20$ kHz) and six different values of ν_{RF} (36, 60, 78, 104, 125, and 178 kHz) were used for conversion. The conversion pulses were optimized according to the rules described in the previous section, yielding a wide range of experimental conditions. In the case of CW irradiation, the optimization included τ_2. In experiments that utilize direct TQC → SQC transfer (schemes I, II, IV, and IV′) with CW irradiation, two intensities were measured for each value of ν_{RF}. As explained earlier, these schemes produce a local intensity maximum at a small value of τ_2. The fact that the optimum values of τ_2 are inversely proportional to ν_{RF} is consistent with this transfer being due to a nutation process. A second maximum represents the RIACT case, with the optimum τ_2 being on the order of $\tau_R/4$. The RIACT effect has not been observed for scheme III, as it is the only approach that does not directly utilize the TQC → SQC conversions. As expected, the optimized values of τ_2 are slightly longer for this scheme. In the FAM-1 method, the efficiency was maximized versus τ_{AM}, while using a constant value of $n = 3$. In all, 80 3QMAS experiments were performed, with the values of τ_2 and τ_{AM} as given in Table 1. Note that common values of τ_2 (or τ_{AM}) are given for schemes I, II, IV, and IV′, as they responded similarly to the tuning procedure.

In agreement with previous studies (*12*), the efficiency of conversion via nutation strongly depends on the ratio between ν_Q and ν_{RF}. The signal intensity increased with increasing ν_{RF} in the entire range shown in Fig. 5 (36 kHz $\leq \nu_{RF} \leq$ 178 kHz or $4.2 \geq \nu_Q/\nu_{RF} \geq 0.84$). Additional simulations showed that for $RbNO_3$ the efficiency plateaus around $\nu_{RF} = 180$ kHz and declines at values exceeding 200 kHz. Two experiments performed using schemes III and IV with the maximum available RF field (200 kHz) were consistent with these predictions (not shown). The dotted lines in Fig. 5a show that remarkably high conversion was observed for the RIACT method, especially with moderate values of ν_{RF}. The data confirm that the RIACT transfer is less sensitive than nutation to the ratio ν_Q/ν_{RF}.

Figure 5b shows that FAM-1 performs very well for all ν_{RF} values used in this work. It is more efficient than CW nutation and RIACT with schemes II, IV, and IV′ and comparable to RIACT with scheme I. Surprisingly, it also performed very well with scheme III, although it was less efficient than the CW nutation method at $\nu_{RF} = 178$ kHz. We note that the relative intensities shown here for $\nu_{RF} = 78$ kHz agree to within 15% with those recently reported by Vosegaard *et al.* (*28*), who used the same spin system (^{87}Rb in $RbNO_3$) and $\nu_{RF} = 80$ kHz to compare FAM-1 conversion in schemes equivalent to I, II, IV, and IV′.

The efficiency of conversion should not be used as the only standard when comparing the conversion methods. An important advantage of FAM-1 transfer is its low sensitivity to the value of ν_Q/ν_{RF}. The implications of FAM-1 are therefore as follows: (i) quadrupolar sites with values of C_Q larger than those accessible to the method of CW may be studied; (ii) nuclei with moderate values of C_Q may be probed with relatively moderate RF power; and (iii) the qualitative distortions in MQMAS can be significantly reduced, both in the isotropic

and in the anisotropic dimension. In addition, recently reported experimental data showed that FAM-1 is relatively robust with respect to off-resonance irradiation, especially when compared with RIACT (*18*). It should be mentioned that the use of higher RF fields increases the tolerance to the off-resonance effects in all methods.

Due to the lower sensitivity, only a few efficiency tests were performed with $LiRbSO_4$. We have determined that in schemes III and IV at $\nu_{RF} = 178$ kHz FAM-1 outperformed the CW nutation method by a factor of approximately 2. The FAM-1 sequence used $n = 3$ and yielded the best efficiency at $\tau_{AM} = 0.54$ μs, which is consistent with the larger C_Q value for this compound. Our attempts to collect the RIACT spectra for $LiRbSO_4$ were not successful.

Resolution

As pointed out earlier, the conversion coefficients must satisfy the conditions $|c_{xx}| = |c_{yy}|$ = maximum and $c_{xy} = c_{yx} = 0$ in order to obtain the optimum TQC → SQC conversion (*18*). Clearly, a deviation from these ideal conditions affects the intensity of the observed signal. However, since the timing of the echo formation, as described by Eq. [1], is independent on the orientation of crystallites, it appears unlikely that a deviation from these ideal conditions may affect the resolution. In order to test the observed linewidth in the isotropic dimension, several 3QMAS spectra of $RbNO_3$ and $LiRbSO_4$ were obtained using CW nutation, RIACT, and FAM-1 conversion. The representative lineshapes are shown in Fig. 6. $LiRbSO_4$ was particularly useful in these tests due to exceptional resolution enhancement that MQMAS provided in this well-crystallized sample. The linewidth of ^{87}Rb in $LiRbSO_4$ changed from ~400 ppm in a static sample to 150 ppm under MAS and 1.5 ppm under 3QMAS. As expected, we were unable to detect any significant changes in resolution while switching among different coherence transfer schemes, ν_{RF} frequencies, and conversion methods (CW, FAM-1, and RIACT for $RbNO_3$; CW and FAM-1 for $LiRbSO_4$).

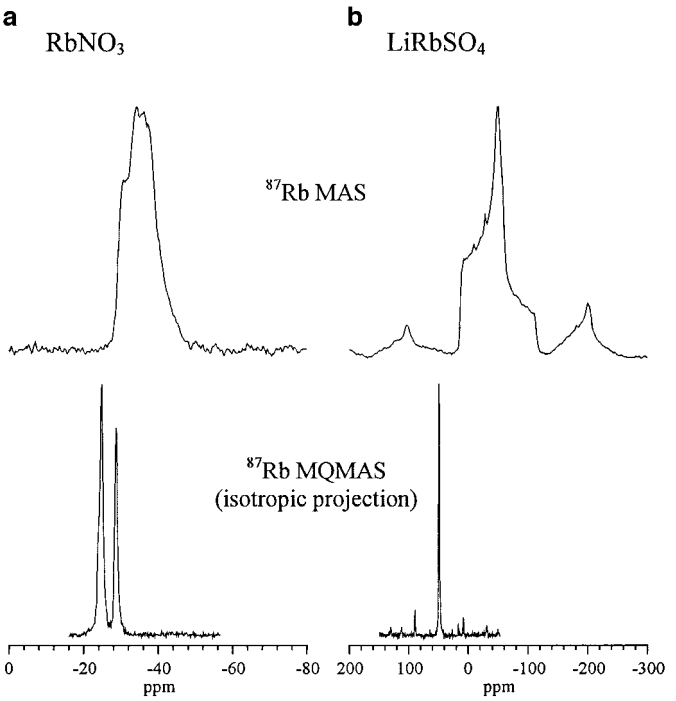

FIG. 6. MAS and MQMAS (isotropic projection) spectra of ^{87}Rb in $RbNO_3$ (a) and $LiRbSO_4$ (b) taken at 130.88 MHz.

CONCLUSION

Our results show that FAM-1 performed better than the nutation and RIACT methods in terms of maximum achievable efficiency and lower sensitivity to the quadrupole frequency. Only in two cases do the CW methods provide comparable efficiency in $RbNO_3$: (i) in the nutation experiments when ν_{RF} matches ν_Q and (ii) in the RIACT experiment with scheme I, as it benefits from simultaneous transfer via echo and antiecho pathways. As is demonstrated in Fig. 5, it is currently possible to obtain MQMAS signal in $RbNO_3$ that exceeds 80% of the intensity achievable by selective excitation of the central transition. Since the efficiency of excitation was around 130% in our experiments, further improvement in TQC → SQC conversion may be possible by using more efficient amplitude and/or frequency modulated schemes (*18*, *19*, *37*, *38*).

Experimentally, the nutation, RIACT and FAM-1 methods yielded similar resolution, regardless of ν_{RF} and C_Q.

With regard to coherence transfer pathways, scheme I exhibits high efficiency with all conversion methods and low sensitivity to ν_Q in the case of RIACT and FAM-1. However, this sequence is not generally suitable for the measurement of pure phase spectra, because it lacks the symmetry needed to balance the contributions from echo and antiecho pathways. In the nutation method, it is possible to lessen this effect by a proper choice of τ_2 (*12*). The RIACT experiment performed with this scheme using strong RF field also provides similar intensities from the echo and antiecho pathways (*22*). In the FAM-1 case, the spectrum is strongly dominated by the echo signal (*18*, *28*) and such a strategy is not suitable. Scheme II performs in a similar way, except that (i) it can be used to generate pure phase spectra through the acquisition of the whole echo, which further increases the sensitivity by up to $\sqrt{2}$, providing that the echo is not strongly affected by homogeneous interactions, and (ii) these spectra do not require shearing.

The *z*-filter method (scheme III) easily provides pure phase spectra. This scheme, when used with a short CW pulse, performed very well at 178 kHz yielding over 60% efficiency in $RbNO_3$. Thus, the *z*-filter method with CW nutation offers an attractive strategy in MQMAS when $\nu_Q/\nu_{RF} \cong 1$. A major

shortcoming of this scheme is that it suffers from high sensitivity to ν_Q.

The $0 \rightarrow \pm 3 \rightarrow \pm 1 \rightarrow 0 \rightarrow -1$ pathway (scheme IV) yields pure phase spectra that do not require shearing, but is the least efficient. It performs better with FAM-1, especially at lower ν_{RF}. Similarly to scheme II, this method can be improved by implementing the acquisition of the whole echo (scheme IV′) when irreversible T_2 effects are not too severe.

In summary, scheme II with FAM-1 conversion is the most successful implementation of the MQMAS experiment for spin-$\frac{3}{2}$ nuclei in a wide range of ν_{RF} values that satisfy the condition $\nu_{RF} < \nu_Q$. When very high ν_{RF} fields are available, scheme II with "brute force" excitation via nutation can be advised. Additional increases in sensitivity can be achieved by "recycling" the converted magnetization in the t_2 dimension using the so-called Carr–Purcell–Meiboom–Gill MQMAS experiment (*29*, *39*) and by improving the methods for numerical analysis of data. For spin-$\frac{5}{2}$ nuclei, FAM-1 conversion sequence should be replaced with double frequency sweep (*38*) or FAM-2 (*40*), and time domains in scheme II should be redefined accordingly.

ACKNOWLEDGMENTS

The authors thank Drs. B. C. Gerstein and S. Vega for valuable discussions. This research was supported at Ames Laboratory by the U.S. Department of Energy, Office of Basic Energy Sciences, Division of Chemical Sciences, under Contract W-7405-Eng-82, and at the University of Lille by the CNRS and the Nord-Pas de Calais Region.

REFERENCES

1. L. Frydman and J. S. Harwood, *J. Am. Chem. Soc.* **117,** 5367 (1995).
2. A. Medek, J. S. Harwood, and L. Frydman, *J. Am. Chem. Soc.* **117,** 12779 (1995).
3. A. Samoson, E. Lipmaa, and A. Pines, *Mol. Phys.* **65,** 1013 (1988).
4. K. T. Mueller, B. Q. Sun, G. C. Chingas, J. W. Zwanziger, T. Terao, and A. Pines, *J. Magn. Reson.* **86,** 470 (1990).
5. C. Fernandez and J.-P. Amoureux, *Chem. Phys. Lett.* **242,** 449 (1995).
6. P. Sarv, B. Wichterlová, and J. Čejka, *J. Phys. Chem.* **102,** 1372 (1998).
7. D. P. Lang, A. Bailly, M. Pruski, J.-P. Amoureux, C. Huguenard, M. Haouas, C. Gerardin, F. Taulelle, T. Loiseau, and G. Ferey, *J. Am. Chem. Soc.* **121,** 12148 (1999).
8. S. J. Hwang, C. Fernandez, J.-P. Amoureux, J. W. Han, J. Cho, S. W. Martin, and M. Pruski, *J. Am. Chem. Soc.* **120,** 7337 (1998).
9. S. Wang and J. Stebbins, *J. Non-Cryst. Solids* **231,** 286 (1998).
10. S. R. Jansen, H. T. Hintzen, R. Metselaar, J. W. de Haan, L. J. M. van de Ven, A. P. M. Kentgens, and G. Nachtegaal, *J. Phys. Chem.* **102,** 5969 (1998).
11. D. Massiot, R. Conanenc, W. Feldmann, R. Marchand, and Y. Laurent, *Inorg. Chem.* **35,** 4957 (1996).
12. J.-P. Amoureux, C. Fernandez, and L. Frydman, *Chem. Phys. Lett.* **259,** 347 (1996).
13. M. J. Duer and C. Stourton, *J. Magn. Reson.* **124,** 189 (1997).
14. L. Marinelli, A. Medek, and L. Frydman, *J. Magn. Reson.* **132,** 88 (1998).
15. S. Ding and C. A. McDowell, *J. Magn. Reson.* **135,** 61 (1998).
16. J.-P. Amoureux, M. Pruski, D. P. Lang, and C. Fernandez, *J. Magn. Reson.* **131,** 170, 1998.
17. P. K. Madhu, A. Goldbourt, L. Frydman, and S. Vega, *Chem. Phys. Lett.* **307,** 41 (1999).
18. P. K. Madhu, A. Goldbourt, L. Frydman, and S. Vega, *J. Phys. Chem.* **112,** 2377 (2000).
19. A. P. M. Kentgens and R. Verhagen, *Chem. Phys. Lett.* **300,** 435 (1999).
20. S. Vega and Y. Naor, *J. Chem. Phys.* **75,** 75 (1981).
21. L. Delevoye, Ph.D. Thesis, University of Lille, France, 1998.
22. T. Charpentier, Ph.D. Thesis, Université de Paris Sud, France, 1998.
23. G. Wu, D. Rovnyak, and R. G. Griffin, *J. Am. Chem. Soc.* **118,** 9326 (1996).
24. A. Vega, *J. Magn. Reson.* **96,** 50 (1992).
25. D. Massiot, B. Touzo, D. Trumeau, J. P. Coutures, J. Virlet, P. Florian, and P. J. Grandinetti, *Solid State NMR* **6,** 73 (1996).
26. S. P. Brown and S. Wimperis, *J. Magn. Reson.* **128,** 42 (1997).
27. J.-P. Amoureux, C. Fernandez, and S. Steuernagel, *J. Magn. Reson. A* **123,** 116 (1996).
28. T. Vosegaard, P. Florian, P. J. Grandinetti, and D. Massiot, *J. Magn. Reson.* **143,** 217 (2000).
29. F. H. Larsen and N. C. Nielsen, *J. Phys. Chem. A* **103,** 10825 (1999).
30. M. Hanaya and R. K. Harris, *J. Phys. Chem.* **101,** 6903 (1997).
31. Crystalline $LiRbSO_4$ was grown at 313 K by means of slow evaporation of aqueous solution containing stoichiometric proportion of Rb_2SO_4 and $Li_2SO_4 \cdot H_2O$. The sample was kindly provided by Dr. H. J. Kim.
32. G. Wu, D. Rovnyak, B. Sun, and R. G. Griffin, *Chem. Phys. Lett.* **249,** 210 (1996).
33. S. P. Brown and S. Wimperis, *J. Magn. Reson.* **124,** 279 (1997).
34. P. J. Grandinetti, J. H. Baltisberger, A. Llor, Y. K. Lee, U. Werner, M. A. Eastman, and A. Pines, *J. Magn. Reson. A* **103,** 72 (1993).
35. S. P. Brown, S. J. Heyes, and S. Wimperis, *J. Magn. Reson. A* **119,** 280 (1996).
36. J.-P. Amoureux, C. Fernandez, and Y. Dumazy, *J. Chim. Phys.* **2,** 1939 (1995).
37. A. Goldbourt, P. K. Mahdu, S. Kababya, and S. Vega, *Solid State NMR,* in press.
38. D. Iuga, H. Schafer, R. Verhagen, and A. P. M. Kentgen, *J. Magn. Reson.* **147,** 192 (2000).
39. T. Vosegaard, F. H. Larsen, H. J. Jakobsen, P. D. Ellis, and N. C. Nielsen, *J. Am. Chem. Soc.* **119,** 9055 (1997).
40. A. Goldbourt, P. K. Mahdu, and S. Vega, *Chem. Phys. Lett.* **320,** 448 (2000).